Journal of Power Sources 195 (2010) 461–465

Contents lists available at ScienceDirect

Journal of Power Sources

journal homepage: www.elsevier.com/locate/jpowsour

Short communication

Development of Pd and Pd–Co catalysts supported on multi-walled carbon nanotubes for formic acid oxidation

D. Morales-Acosta [a], J. Ledesma-Garcia [b], Luis A. Godinez [a], H.G. Rodríguez [a], L. Álvarez-Contreras [c], L.G. Arriaga [a,*]

[a] Centro de Investigación y Desarrollo Tecnológico en Electroquímica, Parque Tecnológico Querétaro, Sanfandila, Pedro Escobedo, C.P. 76703 Querétaro, Mexico
[b] División de Investigación y Posgrado, Facultad de Ingeniería, Universidad Autónoma de Querétaro, Cerro de las Campanas S/N, C.P. 76010, Querétaro, Qro., Mexico
[c] Centro de Investigación en Materiales Avanzados S. C., Complejo Industrial Chihuahua, C.P. 31109, Chihuahua, Chih., Mexico

ARTICLE INFO

Article history:
Received 10 June 2009
Received in revised form 6 August 2009
Accepted 8 August 2009
Available online 15 August 2009

Keywords:
Formic acid electrooxidation
Formic acid fuel cells
Pd–Co alloy
Carbon nanotubes

ABSTRACT

Pd–Co and Pd catalysts were prepared by the impregnation synthesis method at low temperature on multi-walled carbon nanotubes (MWCNTs). The nanotubes were synthesized by spray pyrolysis technique. Both catalysts were obtained with high homogeneous distribution and particle size around 4 nm. The morphology, composition and electrocatalytic properties were investigated by transmission electron microscopy, scanning electron microscopy–energy dispersive X-ray analysis, X-ray diffraction and electrochemical measurements, respectively. The electrocatalytic activity of Pd and PdCo/MWCNTs catalysts was investigated in terms of formic acid electrooxidation at low concentration in H_2SO_4 aqueous solution. The results obtained from voltamperometric studies showed that the current density achieved with the PdCo/MWCNTs catalyst is 3 times higher than that reached with the Pd/MWCNTs catalyst. The onset potential for formic acid electrooxidation on PdCo/MWCNTs electrocatalyst showed a negative shift ca. 50 mV compared with Pd/MWCNTs.

1. Introduction

The electrochemical oxidation of small organic molecules has been widely studied due to their potential utilization as fuel in energy conversion systems. The main reason is related to their low toxicity, facility of storage, handling and primarily their energy density. Moreover, due to their simple molecular structure they should undergo a more straightforward reaction mechanism than other possible organic fuels [1–4].

In this context, formic acid, a non-toxic and non-explosive liquid at room temperature, has shown potential applications in small portable fuel cell applications [5,6]. The mechanism of formic acid electrooxidation on Pt and select Pt-group metal surfaces in acid solution follows the so-called dual pathways dehydrogenation and dehydration [7]. Numerous studies have shown for instance that Pd catalysts accomplish higher activity for formic acid oxidation than Pt [8,9]. Palladium is a metal known for its ability to catalyze CO oxidation and other hydrocarbons as well [10]. It has an electronic configuration identical to platinum and forms a not so strong, bond to most absorbates. The key differences are: Pd-*d*-bands are closer to the cores than platinum, and there is less *d* electron density available for bonding. This leads to weaker interactions with π bonds, which allows unique chemistry to occur. Pd has higher oxidation potential than Pt, and the Pd oxides are more stable [11]. Weak inter-atomic bonds between palladium atoms compared to platinum or nickel lead to easy formation of subsurface species, whose role is still uncertain. Also, palladium has a very similar lattice constant to that of platinum [11].

On the other hand, it is well known that the type of carbon support affects the performance and stability of the catalysts. Carbon supported palladium catalysts have become a very important area in DFAFC (direct formic acid fuel cell) catalyst research in recent years, showing good activity along with the potential for more efficient palladium metal utilization and lower metal loadings [12–17]. In this context, Ha et al. synthesized Pd particles dispersed on Vulcan XC-72® carbon support and the results were compared with those obtained from pure palladium in DFAFC [12]. Even in the light of these and other, it is clear that in order to achieve an improved performance in terms of activity and stability of the Pd catalysts, a promising approach consists in the addition of metal or metal oxide promoters [18]. Carbon nanotubes (CNTs) are of interest as catalyst supports for applications in fuel cells due to their unique electrical and structural properties [19,20]. Multi-walled carbon nanotubes (MWCNTs) have been used as the support of the cathode electrocatalyst and showed a better performance in DEFCs (direct

* Corresponding author. Tel.: +52 442 211 6069; fax: +52 442 211 6000.
E-mail address: larriaga@cideteq.mx (L.G. Arriaga).

0378-7753/$ – see front matter © 2009 Elsevier B.V. All rights reserved.
doi:10.1016/j.jpowsour.2009.08.014

ethanol fuel cells) due to the higher nanoparticle dispersion than that electrocatalysts supported on carbon black [21–25].

In this study MWCNTs were prepared by the spray pyrolysis technique and used to supporting Pd-based electrocatalysts. Some authors have supported alloy catalysts by low temperature aqueous route on high surface area carbon with nanometer size particles, stability and superior electrocatalytic properties [26,27]. In this work, the novel materials were synthesized by impregnation method on MWCNTs at low temperature. The physicochemical properties of Pd-electrocatalysts were evaluated by transmission electron microscopy (TEM), scanning electron microscopy coupled to energy dispersive X-ray (SEM–EDX) and X-ray diffraction (XRD). The electrooxidation of 0.1 M formic acid was investigated in order to show the high catalytic activity of our materials and a comparison with the performance of the Pd/XC-72 commercial electrocatalyst was done.

2. Experimental

2.1. Synthesis and funcionalization of MWCNTs

MWCNTs were synthesized using the spray pyrolysis technique. The detailed procedure of preparation has already been reported [28]. The MWCNTs were cleaned by immersion in concentrated HNO_3 in an ultrasonic bath for 1 h. After that, they were refluxed for 12 h at 80 °C. The solution was filtered and washed with plenty of distilled water. In order to promote their funcionalization, the MWCNTs were immersed in a HNO_3/H_2SO_4 (1:4, v/v) solution for 5 h at 60 °C under refluxing and stirred conditions. Later, the wet powder was washed with deionized water until the pH of the filtrated solution was 7. Finally, the powder obtained was dried overnight at 60 °C.

2.2. Preparation and physicochemical characterization of Pd and Pd–Co catalysts

Pd-based catalysts were prepared by the impregnation on MWCNTs and reduced by the action of $NaBH_4$. The procedure for the synthesis of Pd/MWCNTs was as follows: MWCNTs were first dispersed in deionized water by treated in an ultrasonic bath for 60 min. After that, the nanotubes were added into $(NH_4)_2PdCl_6$ (Stream Chemicals, 99%) aqueous solution. $NaBH_4$ (Sigma–Aldrich, 98.5%) was slowly dropped into this mixture and vigorously stirred for 1 h. The molar ratio between the metal and the reducing agent was 1:5. The resulting solution was filtered, washed and dried overnight at 60 °C. The same method for preparation of PdCo/MWCNTs was carried out. In this case however, previous to the $NaBH_4$ addition to the mixture of $(NH_4)_2PdCl_6$-MWCNTs, $CoN_2O_6{\cdot}6H_2O$ (Acros Organic, 99%) was added to the aqueous solution. In order to remove the excess of cobalt in PdCo/MWCNTs, a treatment with 0.1 M HCl was accomplished.

The obtained powders were characterized by X-ray diffraction (XRD) measurements on an X-pert MPD Phillips Diffractometer using Cu Kα radiation operating at 43 kV and 30 mA. The peak profile of the (2 2 0) reflection in the face-centered cubic structure was obtained by using the Marquardt algorithm and used to calculate the crystallite size utilizing the Debye–Scherrer equation [29]. A JEOL JSM 5800-LV scanning electron microscope (SEM) on the other hand, was used for SEM–energy dispersive X-ray (EDX) analysis of the catalysts. The morphology of catalysts was investigated using a Philips Model CM200 transmission electron microscope (TEM) operated at 200 kV.

2.3. Half-cell experiments

Electrochemical experiments consisted in cyclic voltammetry (CV) and linear sweep voltammetry (LSV) using a BAS Epsilon Potentiostat/Galvanostat (Bioanalytical Systems). A glassy carbon electrode (3 mm diameter) was used as working electrode in a standard three-electrode glass cell, using a Hg/Hg_2SO_4 electrode and a Pt wire as reference and counter electrode, respectively. Potentials in the text are referred to the NHE (normal hydrogen electrode).

The working electrode, which was used as substrate of catalyst inks, was prepared by polishing until a mirror-finished with 0.05 μm alumina powder followed by rinsing in water. Later, 1 mg of catalyst was dispersed in 200 μl of isopropyl alcohol in an ultrasonic bath for 40 min; afterwards, 20 μl of Nafion® 5% solution were added and continuously stirred for 20 min. Two aliquots of 1.5 μL of the electrocatalytic ink were deposited onto glassy carbon disks and dried under a nitrogen flow. For comparison, a commercial Pd/XC-72 catalyst was used (Electrochem®, 10 wt.%). The electrode was also prepared according to the procedure described above.

All electrolytes were prepared with deionized water ($\rho \geq 18\,M\Omega\,cm$). The formic acid electrooxidation was investigated in 0.1 M in 0.5 M H_2SO_4, which was employed as electrolyte. Before each experiment, the electrode was cycled for 5 min at 20 mV s^{-1} between 0.08 and 1.2 V in 0.5 M H_2SO_4 under N_2 atmosphere in order to clean the surface. Afterwards, CV experiments were carried out in the presence of 0.1 M formic acid. LSV curves of 0.1 M formic acid were recorded at different scan rates (20, 40, 60, 80 and 100 mV s^{-1}). The experiments were carried out under research-grade N_2 atmosphere (Infra, 99.999% pure) and the temperature was kept in all cases at 30 °C.

3. Results and discussion

3.1. Physicochemical characterization

X-ray diffraction patterns collected from Pd/MWCNTs and PdCo/MWCNTs catalysts are presented in Fig. 1. The maximum peak located at 26° corresponds to the graphite (0 0 2) plane of MWCNTs support [30]. The other principal peaks exhibit the characteristics of a single face-centered-cubic (fcc) crystallographic structure of Pd (JCPDS, Card No. 5-681), corresponding to the planes (1 1 1), (2 0 0), (2 2 0) and (3 1 1) located at 40°, 47°, 68° and 82°, respectively. Although not exists an obvious shift of these four diffraction peaks for the PdCo material with respect to the corresponding peaks in the Pd catalyst, a lattice contraction caused by the incorporation of Co into the Pd fcc structure is revealed by a lower value in the lattice parameter of PdCo catalyst. This Pd lattice compression or reduction of bond lengths between metals can be induced by the

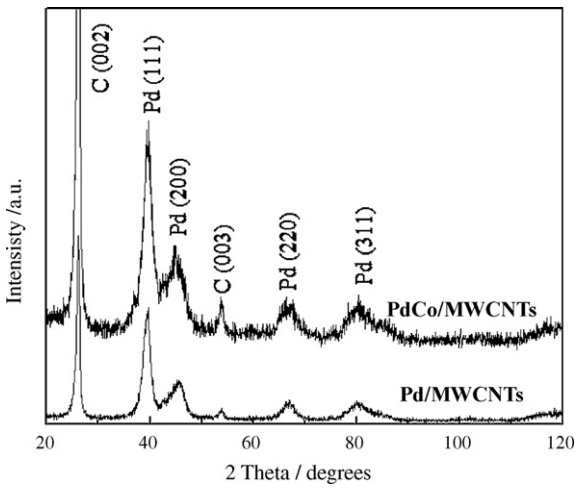

Fig. 1. XRD patterns of Pd/MWCNTs and PdCo/MWCNTs.

Table 1
Physicochemical and electrochemical characteristics of PdCo/MWCNTs, Pd/MWCNTs and Pd/XC-72 catalysts.

	Pd/XC-72	Pd/MWCNTs	PdCo/MWCNTs
Composition Pd:Co/% (EDX)	–	100:0	60:40
Mean particle size/nm (XRD)	7.5	3.5	3.9
Mean particle size/nm (TEM)	–	4.0	4.2
Lattice parameter/nm	0.389	0.396	0.395
$S/m^2\ g^{-1}$	41.5	66	57.8

alloy formation between Pd and Co [31–34]. The values of lattice parameter of Pd and PdCo catalysts are listed in Table 1.

The average crystallite size of the two catalysts was estimated from diffractograms using the Scherrer equation applied to the (2 2 0) peak [33]. Particle dimensions of 3.5 and 3.9 nm were obtained in this way for Pd and Pd–Co catalysts, respectively.

On the other hand, while the low magnification SEM image presented in Fig. 2A shows the distribution of Pd–Co nanoparticles on the MWCNTs, Fig. 2B illustrates their corresponding elemental composition obtained by EDX measurements. The resulting values are also presented in Table 1.

TEM micrographs and particle size histograms of (A) Pd and (B) Pd–Co materials shown in Fig. 3 reveal a good dispersion of nanoparticles on the surface of MWCNTs with a relative narrow particle size distribution, the mean particle diameters are ca. 4.0 and 4.2 nm, respectively. While these values are close to those obtained from XRD measurements, they are also similar to the particle size previously reported for materials synthesized without the use of stabilizer agents or thermal treatment [35].

3.2. Electrochemical characterization

Fig. 4 compares the electrochemical responses of Pd/MWCNTs and PdCo/MWCNTs in 0.5 M H_2SO_4 measured in the potential range between 0 and 1.3 V vs NHE. The typical voltammetric curve of Pd in acid media was observed; whereas Pd–Co catalyst presents a CV profile with significant variations. The current density between 0 and 0.3 V range was lower for Pd–Co than that recorded for pure Pd, suggesting an inhibition of the hydrogen/desorption on Pd or oxygenated species formation at Co-sites. In the double layer region (0.3–0.6 V approximately) no oxygenated species formation are

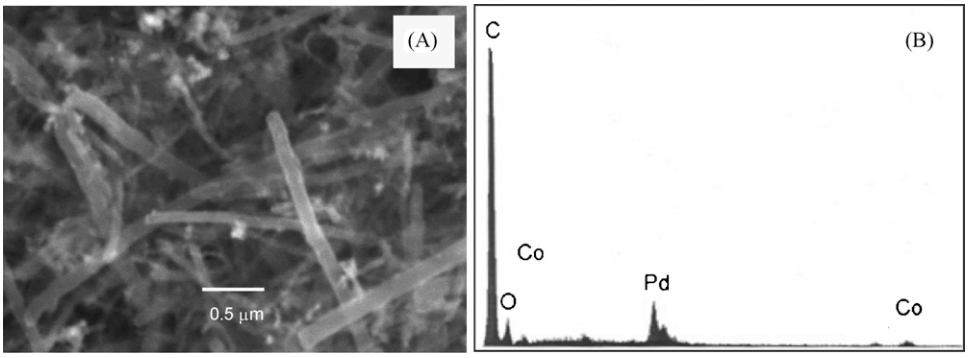

Fig. 2. (A) SEM at 35,000× and (B) EDX of PdCo/MWCNTs.

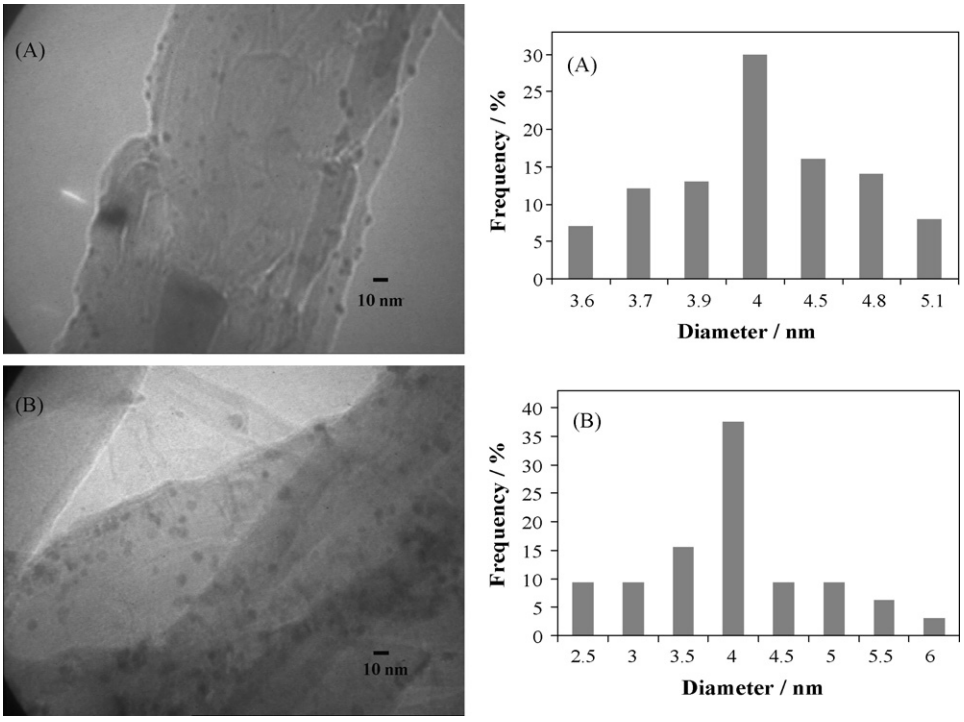

Fig. 3. TEM images and corresponding particle size histogram of (A) Pd/MWCNTs and (B) PdCo/MWCNTs.

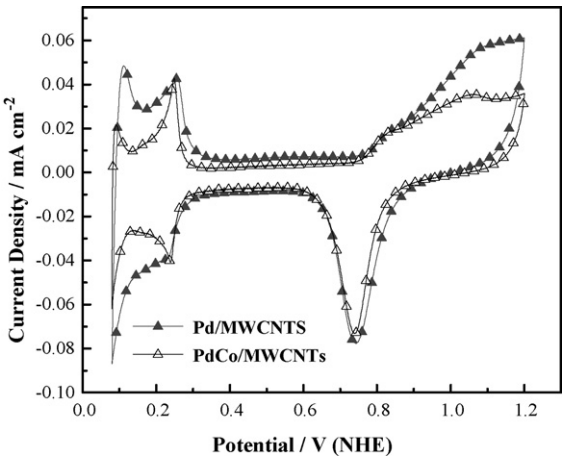

Fig. 4. Cyclic voltammograms of Pd/MWCNTs and PdCo/MWCNTs electrodes in N_2-satured 0.5 M H_2SO_4. Scan rate 20 mV s^{-1} at 30 °C.

observed, only to high potentials (1 V) where there is no practical fuel cell interest.

According to the cyclic voltammograms presented in Fig. 4, the electroactive surface area (ESA) of Pd and Pd–Co catalysts was calculated from the density of charge associated to the reduction of a full monolayer of Pd oxides [36]. Specific surface area (S/m^2 g^{-1}) was then, estimated from the ESA:Pd loading ratio [37] for each electrode and compared with a Pd/XC-72. The values are presented in Table 1. The S obtained for MWCNTs-supported materials is higher compared to commercial Pd. This is attributed to the smaller metal particles supported on MWCNTs with a better distribution in comparison with Vulcan.

The electrocatalytic properties of the Pd/MWCNTs and PdCo/MWCNTs for formic acid electrooxidation were investigated in 0.1 M HCOOH + 0.5 M H_2SO_4 aqueous solution by cyclic voltammetry. Fig. 5 shows the corresponding response measured at 20 mV s^{-1} between 0.08 and 1.2 V. For comparison, cyclic voltammogram of formic acid electrooxidation at the commercial Pd/XC-72 is also presented in Fig. 5. It is clear that a peak associated with the formic acid oxidation process was recorded in both forward and reverse scans. This behavior is typically observed for Pd catalysts [38]. The electrooxidation peak of formic acid was observed in the forward scan at 0.28, 0.32 and 0.38 V for PdCo/MWCNTs, Pd/MWCNTs and Pd/XC-72, respectively. The onset potential for formic acid electrooxidation on PdCo/MWCNTs electrocatalyst showed a negative shift. This indicates that the Pd–Co based material favors formic acid electrooxidation as compared to Pd. Additionally, the anodic potential for this reaction on PdCo/MWCNTs is compared with another work that uses a Pd–Co supported on Vulcan, our result shows a more negative shift that than obtained from the reference 0.28 V and 0.42 V vs NHE, respectively [26]. This behavior could be attributed to the atomic optimization of Pd–Co relationship.

Furthermore, it can seen from Fig. 5 that the maximum current density associated to formic acid electrooxidation determined at 0.28 V on the catalysts has the following order: PdCo/MWCNTs (107 mA cm^{-2}) > Pd/MWCNTs (35.6 mA cm^{-2}) > Pd/XC-72 (24.8 mA cm^{-2}). These results reveal that the anodic peak current density obtained by using PdCo/MWCNTs as catalyst is 3 and 4.3 times higher than those observed when Pd/MWCNTs and Pd/XC-72 were employed, respectively. The difference could be attributed to a better dispersion of metallic nanoparticles with a lower particle size achieved with the MWCNTs-supported materials. Additionally, it is evident that the interaction between Pd and Co in the PdCo/MWCNTs catalyst facilitates the oxidation reaction of formic acid, probably due to a direct oxidation pathway to CO_2. In this context, previous authors have suggested that the addition of Co avoids the adsorption of reactive intermediates during the oxidation of formic acid, preventing the accumulation of poisoning-intermediates. Therefore, more Pd active sites are available for the direct decomposition of formic acid through the direct pathway [26].

Furthermore, in order to evaluate the stability of PdCo-MWCNTs based catalyst, chronoamperometry experiments at 0.3 V vs NHE were carried out in the presence of 0.1 M HCOOH in 0.5 M H_2SO_4 aqueous solution. Fig. 6 shows the current density behavior for the formic acid oxidation as a function of the time. It can be observed that the maximum current density obtained is near to 100 mA cm^{-2} on PdCo/MWCNTs catalyst, after that, decrease in an exponential way and remains practically constant. This result demonstrates that PdCo/MWCNTs electrode has electrocatalytic stability for the formic acid oxidation.

The effect of scan rate on the behavior of formic acid oxidation on PdCo/MWCNTs and Pd/MWCNTs electrodes was investigated by mean of LSV measurements. In Fig. 7 the current density was plotted as a function of the scan rate ($v^{1/2}$). The result clearly reveals that the peak current density associated to the formic acid electrooxidation increases linearly with the scan rate. This behavior indicates that the electrocatalytic process under study is controlled by diffusion [39]. Furthermore, the current density value recorded for the

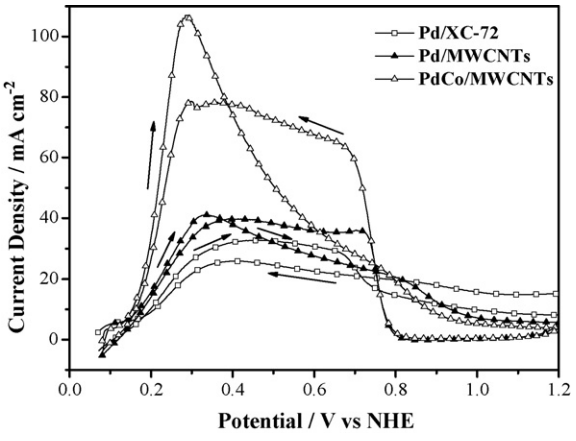

Fig. 5. Cyclic voltammograms obtained on the Pd/MWCNTs, PdCo/MWCNTs and Pd/XC-72 electrodes in 0.1 M HCOOH + 0.5 M H_2SO_4 aqueous solutions at 20 mV s^{-1}. The measurements were carried out at 30 °C in a saturated N_2 environment.

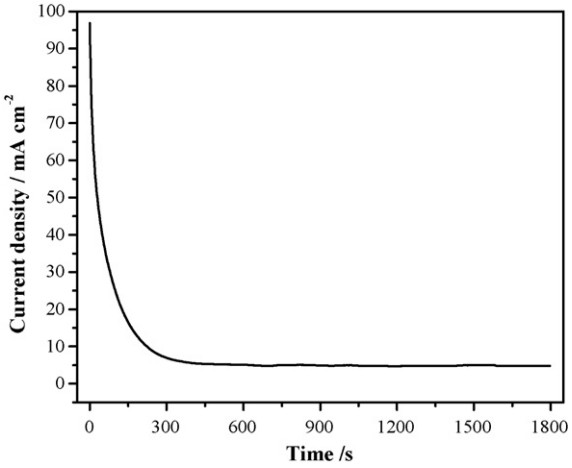

Fig. 6. Chronoamperometric curve on PdCo/MWCNTs electrode at 0.3 V vs NHE for 1800 s in the presence of 0.1 M HCOOH in 0.5 M H_2SO_4.

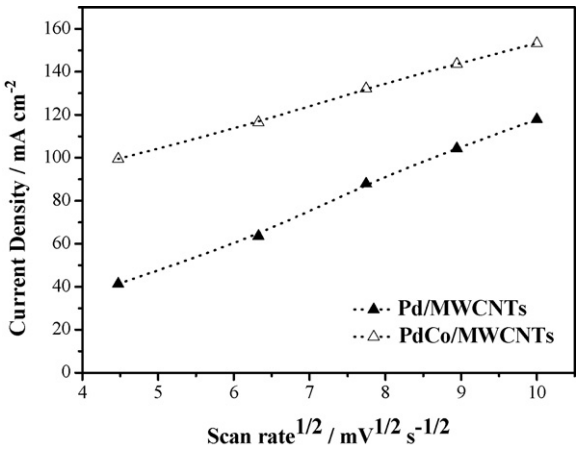

Fig. 7. Plot of the anodic current density of 0.1 M formic acid in 0.5 M H_2SO_4 vs the scan rate, using Pd/MWCNTs and PdCo/MWCNTs as electrocatalysts. LSV experiments were carried out at 30 °C in a saturated N_2 environment.

PdCo/MWCNTs is larger than that of the Pd/MWCNTs electrode. This observation confirms the results above described.

4. Conclusions

In summary PdCo/MWCNTs and Pd/MWCNTs were prepared at low temperature impregnation method and physicochemically characterized by XRD, SEM–EDX and TEM techniques. The particle size obtained by this synthesis procedure was around 4 nm. The electrocatalytic properties of the synthesized materials were evaluated for the formic acid electrooxidation. PdCo/MWCNTs exhibit good stability in acid media and higher current density and more negative anodic potential associated to this reaction than that achieved with Pd/MWCNTs and Pd/XC72 electrocatalysts: 3 and 4.3 times, as well as, 50 and 100 mV, respectively. Furthermore, this shift of potential was 140 mV larger than PdCo-carbon based materials. Specific surface area obtained from PdCo and Pd supported on MWCNTs is higher than that obtained with Pd supported on Vulcan. These interesting nano-structured materials offer potential possibilities of application as electrocatalysts composites in direct formic acid fuel cells.

Acknowledgments

The authors gratefully acknowledge financial support from the Mexican Council for Science and Technology (CONACyT, Grant 61067). We also thank to E. Torres, K. Campos and I. Alonso for support with XRD, SEM and TEM measurements. J.L.-G. thanks to Facultad de Ingenieria UAQ-FIFI 2009 for financial support.

References

[1] B.D. McNicol, D.A.J. Rand, K.R. Williams, J. Power Sources 83 (1999) 15.
[2] S. Ha, R. Larsen, Y. Zhu, R.I. Masel, Fuel Cells 4 (2004) 337.
[3] C. Rice, S. Ha, R.I. Masel, P. Waszczuk, A. Wieckowski, T. Barnard, J. Power Sources 111 (2002) 83.
[4] H. Li, G. Sun, Q. Jiang, M. Zhu, S. Sun, Q. Xin, Electrochem. Commun. 9 (2007) 1410.
[5] B. Liu, H.Y. Li, L. Die, X.H. Zhang, Z. Fan, J.H. Chen, J. Power Sources 186 (2009) 62.
[6] S.Y. Wang, N. Kristian, S.P. Jiang, X. Wang, Electrochem. Commun. 10 (2008) 961.
[7] R. Parsons, T. VanderNoot, J. Electroanal. Chem. 257 (1988) 9.
[8] Z. Liu, L. Hong, M.P. Tham, T.H. Lim, H. Jiang, J. Power Sources 161 (2006) 835.
[9] F.J. Vidal-Iglesias, J. Solla-Gullon, E. Herrero, A. Aldaz, J.M. Feliu, J. Appl. Electrochem. 36 (2006) 1207.
[10] F. Garin, Catal. Today 89 (2004) 255.
[11] W. Vielstich, A. Lamm, H.A. Gasteiger (Eds.), Handbook of Fuel Cells: Fundamentals Technology and Application, Wiley, NJ, 2003.
[12] S. Ha, R. Larsen, R.I. Masel, J. Power Sources 144 (2005) 28.
[13] Z.L. Liu, L. Hong, M.P. Tham, T.H. Lim, H.X. Jiang, J. Power Sources 161 (2006) 831.
[14] L.L. Zhang, T.H. Lu, J.C. Bao, Y.W. Tang, C. Li, Electrochem. Commun. 8 (2006) 1625.
[15] L.L. Zhang, Y.W. Tang, J.C. Bao, T.H. Lu, C. Li, J. Power Sources 162 (2006) 177.
[16] R. Larsen, S. Ha, J. Zakzeski, R.I. Masel, J. Power Sources 157 (2006) 78.
[17] X.G. Li, I.M. Hsing, Electrochim. Acta 51 (2006) 3477.
[18] R. Larsen, j. Zakzeski, R.I. Masel, Electrochem. Solid-State Lett. 8 (2005) A291.
[19] B. Coq, J.M. Planeix, V. Brotons, Appl. Catal. A 173 (1998) 175.
[20] P. Serp, M. Corrias, P. Kalck, Appl. Catal. A 253 (2003) 337.
[21] W.Z. Li, C.H. Liang, J.S. Qiu, W.J. Zhou, H.M. Han, Z.B. Wei, G.Q. Sun, Q. Xin, Carbon 40 (2002) 787.
[22] R.P. Raffaelle, B.J. Landi, J.D. Harris, S.G. Bailey, A.F. Hepp, Mater. Sci. Eng. B 116 (2005) 233.
[23] T. Matsumoto, T. Omatsu, H. Nakano, K. Arai, Y. Nagashima, E. Yoo, T. Yamazaki, M. Kijima, H. Shimizu, Y. Takasawa, J. Nakamura, Catal. Today 90 (2004) 277.
[24] W.Z. Li, C.H. Liang, W.J. Zhou, J.S. Qiu, Z.H. Zhou, G.Q. Sun, Q. Xin, J. Phys. Chem. B 1076 (2003) 292.
[25] X.S. Zhao, W.Z. Li, L.H. Jiang, W.J. Zhou, Q. Xin, B.L. Yi, G.Q. Sun, Carbon 42 (2004) 3251.
[26] X. Wang, Y. Xia, Electrochem. Commun. 10 (2008) 1644.
[27] L. Xiong, A.M. Kannan, A. Manthiram, Electrochem. Commun. 4 (2002) 898.
[28] V. Baglio, A. Di Blasi, C. D'Urso, V. Antonucci, A.S. Aricò, R. Ornelas, D. Morales-Acosta, J. Ledesma-Garcia, L.A. Godinez, L. Alvarez-Contreras, L.G. Arriaga, J. Electrochem. Soc. 155 (2008) B829.
[29] A.R. West, Solid State Chemistry and Its Applications, first ed., Wiley, New York, 1984.
[30] S.K. Cui, D.J. Guo, J. Colloid Interface Sci. 333 (2009) 300.
[31] T. Toda, H. Igarashi, H. Uchida, M. Watanabe, J. Electrochem. Soc. 146 (1999) 3750.
[32] L. Zhang, K. Lee, J. Zhang, Electrochim. Acta 52 (2007) 7964.
[33] X. Li, Q. Huang, Z. Zou, B. Xia, H. Yang, Electrochim. Acta 53 (2008) 6662.
[34] L. Zhang, K. Lee, J. Zhang, Electrochim. Acta 52 (2007) 3088.
[35] Y. Zhu, Y. Kang, Z. Zou, Q. Zhou, J. Zheng, B. Xia, H. Yang, Electrochem. Commun. 10 (2008) 802.
[36] M.W. Breiter, J. Electroanal. Chem. 81 (1977) 275.
[37] S.D. Thompson, L.R. Jordan, M. Forsyth, Electrochim. Acta 46 (2001) 1657.
[38] S. Yang, X. Zheng, H. Mi, X. Ye, J. Power Sources 175 (2008) 26.
[39] A.J. Bard, L. Faulkner, Electrochemical Methods: Fundamentals and Applications, Wiley, New York, 1980.